Studying Townsend and glow modes in an atmospheric-pressure DBD using mass spectrometry

Author(s) Kirsty McKay[1], David Donaghy[1], Feng He[2] and *James W Bradley[1]

---

1 Dr. Kirsty McKay.
Department of Electrical Engineering and Electronics, The University of Liverpool,
Brownlow Hill, Liverpool, L69 3GJ, UK
E-mail: k.mckay@liverpool.ac.uk

1 Dr. David Donaghy.
Department of Electrical Engineering and Electronics, The University of Liverpool,
Brownlow Hill, Liverpool, L69 3GJ, UK
E-mail: donaghy@liverpool.ac.uk

2 Dr. Feng He.
School of Physics, Beijing Institute of Technology, P.O. Box 327, Beijing 100081, China
E-mail: hefeng@bit.edu.cn

1 Prof. James W Bradley
Department of Electrical Engineering and Electronics, The University of Liverpool,
Brownlow Hill, Liverpool, L69 3GJ, UK
E-mail: jbradley@liverpool.ac.uk

Abstract

Ambient molecular beam mass spectrometry has been employed to examine the effects of the mode of operation and the excitation waveform on the ionic content of a helium-based atmospheric-pressure parallel plate dielectric barrier discharge. By applying 10 kHz microsecond voltage pulses with a nanosecond rise times and 10 kHz sinusoidal voltage waveforms distinctly different glow and Townsend modes were produced, respectively. Results showed a significant difference in the dominant ion species between the two modes. In the Townsend mode molecular oxygen ions, atomic oxygen anions and nitric oxide anions are the most abundant species, however, in the glow mode water clusters ions and hydrated nitric oxygen anions dominate. Several hypotheses are put forward to explain these differences, including low electron densities and energies in the Townsend mode, more efficient ionization of water molecules through penning ionization and charge exchange with

other species in glow mode, and large temperature gradients due to the pulsed nature of the glow mode, leading to more favorable conditions for cluster formation.

1. Introduction

Dielectric barrier discharges (DBD) have become important in a range of applications from materials processing to healthcare [1-3]. At atmospheric pressure DBD's are commonly used in parallel (electrode) plate configuration and can be operated using a variety of waveforms, but other configurations are also often used. For example single or double ring electrodes can be exploited around dielectric tubes to form jets or electrodes can be fixed to either side of a dielectric to create surface discharges [4, 5]. Parallel plate DBD's can operate in a number of modes, for instance in non-uniform filamentary mode where the discharge consists of multiple spatially narrow, short-lived current channels bridging the gap between cathode and anode, or in uniform mode, where the discharge current acts across the whole electrode area once per half cycle [6-8]. The operating mode depends on the specific operating conditions, namely gas type, flow rate, chamber pressure, applied voltage waveform, dielectric electrode material, electrode thickness, and reactor geometry [6].

Here, the ionic chemistry of two distinct homogenous uniform modes of operation are of interest, namely the atmospheric-pressure glow discharge (APGD) and atmospheric pressure Townsend discharge (APTD) modes. For the APGD mode the plasma is formed uniformly once every half cycle of the external voltage, with current densities typically greater than 10 mA/cm^2 per period [9-11]. In the Townsend regime the current density is one to two orders of magnitude lower at approximately 0.1-1 mA/cm^2 [6, 12] and the breakdown is characterized by reduced ionization rates of the gas when compared to APGD or streamer discharges [13, 14].

In recent years, unipolar nanosecond rise-time pulsing and microsecond square wave pulsing techniques have been used to drive DBD's with the aim of increasing the power efficiency of the reactor. The discharge resulting from the falling voltage pulse edge, utilizes the

accumulated surface and space charge left from the rising pulse edge cycle. Hence, no additional energy is required from an external source. These ions are normally partially or totally lost under normal low frequency sine or square waveforms [15, 16]. Previous research has shown that at atmospheric pressure sinusoidal wave excitation leads to the filamentary glow mode for a range of simple and complex gases, while nanosecond rise-times (fast pulsing) can produce uniform (diffuse) glow discharges [9, 10]. However, some studies have shown that at atmospheric pressure sinusoidal excitation can be used to create uniform Townsend mode discharges [17]. Uniform discharges are often characterized using ICCD imaging which allows filaments to be resolved if they exist in the discharge [11, 18-20], however, due to the geometry of certain electrode configurations it is not always possible to perform this imaging. In those cases the current trace is often used to determine whether the discharge is filamentary in nature. The micro discharges in a filamentary discharge are distributed randomly over the entire discharge resulting in a number of current spikes [21], whereas Townsend discharges are relatively uniform and tend to have a smooth current trace [20].

The study of atmospheric-pressure discharges using molecular beam mass spectrometry (MBMS) has previously been reported, for instance in the diagnosis of micro-plasma jets[22-24], DBD's[25-28] and parallel plate RF discharge [29]. Until now however, there has been no MBMS diagnostic study to compare the ionic make-up of atmospheric-pressure homogeneous DBD's driven in different modes using different driving waveforms. Here, we present a study of a (single dielectric) parallel plate DBD operating in helium and excited using unipolar square-waves and more conventional sinusoidal voltages. The aim of this study was to determine the effect of the operational mode and driving waveform on the type and relative quantity of potentially important ionic species created in the discharge.

2. Experimental Arrangement

The experimental setup is shown in figure 1. The driving electrode consisted of a 2 cm diameter circular thin copper plate covered with a 6 cm diameter 1.2 mm thick pure alumina dielectric plate (relative permittivity 9.5). The grounded electrode was the metal front cone of the mass spectrometer. The electrode separation was maintained at 0.5 mm during the experiments using ceramic spacers. The copper electrode was electrically connected to either the unipolar square-wave or sine-wave high voltage power supply. The DBD was covered by an airtight chamber with a gas inlet and outlet. Atmospheric-pressure helium (purity of 99.995%) was fed into the chamber via an MKS mass flow controller. The nanosecond square-wave power supply was homemade, consisting of a high voltage DC power supply (EK30P20) and a custom built printed circuit board producing 0~3kV pulses of frequency 10 Hz to 20kHz with rise and fall time of approximately 225 and 400 ns respectively. The sinusoidal wave power source consisted of a TTI TG2000 function generator, a Velleman VPA2350MB audio amplifier and an Amethyst AD7161 transformer. The applied voltage and current flowing in the external circuit were measured using a P6015A Tektronix voltage probe and Pearson 2877 current monitor displayed on a digital oscilloscope (Tektronix DPO 4034B), respectively. The helium gas flow rate was kept constant at 2 slm. The ambient temperature was 20℃ with a relative humidity of the air of 50%.

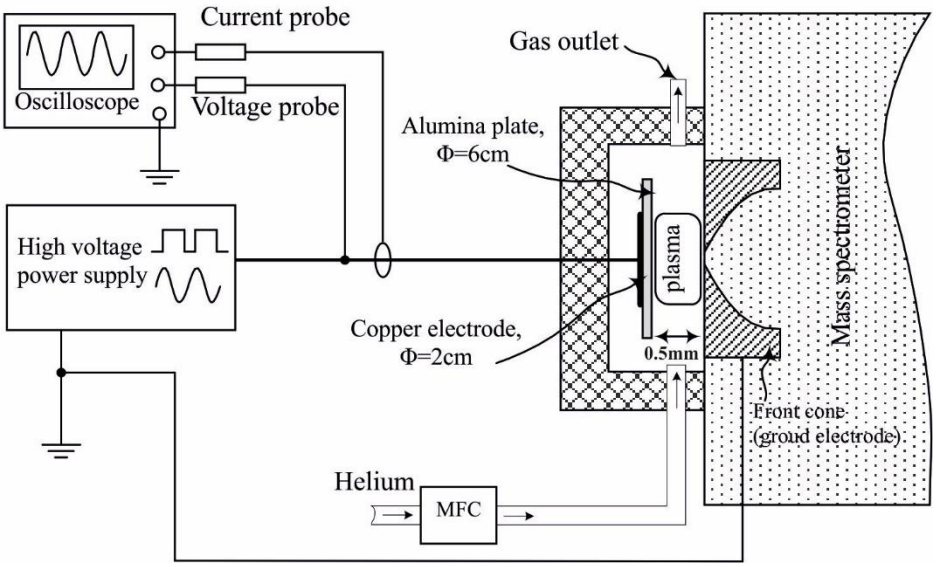

Figure 1. The schematic of the experimental system

To determine the ionic content of the different discharge modes a quadrupole-based molecular beam mass spectrometer system (HPR-60) manufactured by Hiden Analytical Ltd was used. More details of this three stage differentially pumped system can be found in McKay *et. al.* [17, 27]. Since the extraction cone of the mass spectrometer acted as the grounded electrode this allowed ions to be sampled from the plasma without perturbing the discharge itself. The front cone orifice size was 25 µm. The second stage cone was a 400 µm orifice, which was set to have a potential of either -10V or +10V to extract positive or negative ions respectively. The small aperture on the front cone and the low voltage on the second cone prevented penetration of the electric field from the second stage cone behind the extraction cone into the discharge region. The aperture also provides a continuous sheath across the orifice thus preventing plasma penetration into the instrument. This reduced the chances of internal ion production and unwanted ion acceleration [30].

The mass spectrometer was tuned to maximize the signal for ion detection (so called secondary ion mass spectrometry SIMS mode). The MS was operated under the same tuning conditions for both the sinusoidal and pulsed discharges, allowing direct comparison of the

ion chemistry without any correction factor being used. In our study, a detector dwell time of 100 ms was set so all the data points were counted over 1000 periods of the driving waveform to diminish the influence of discontinuous plasma in a DBD. In order to compare the results for different waveforms and different voltages, ions of mass up to 130 amu were scanned with a resolution of 0.2 amu, and averaged over 5 cycles to obtain the relative intensity of each of the mass selected species.

Electrical characterization of the different modes of operation

To produce the glow and Townsend regimes the DBD was driven at a repetition frequency of 10 kHz for both the pulsed and sinusoidal waveforms. For unipolar pulsing the duty ratio was 50%. The peak-to-peak potential across the DBD, V_{pp}, for the sinusoidal and unipolar square pulsing was 0.9 - 1.5 kV and 0.75 - 1.2 kV respectively. The average power dissipated in the discharge over the entire voltage cycle was calculated using the method described by Massines et. al. and Liu et. al.[12, 15, 31], where the externally measured voltage and current were used to calculate the voltage across the discharge gap, V_{gas}, and the instantaneous power as a function of time in the discharge gap.

Typical discharge voltage and current waveforms, measured at the powered electrode, are shown in figure 2 and the corresponding gas voltage and the instantaneous discharge power are shown in figure 3.

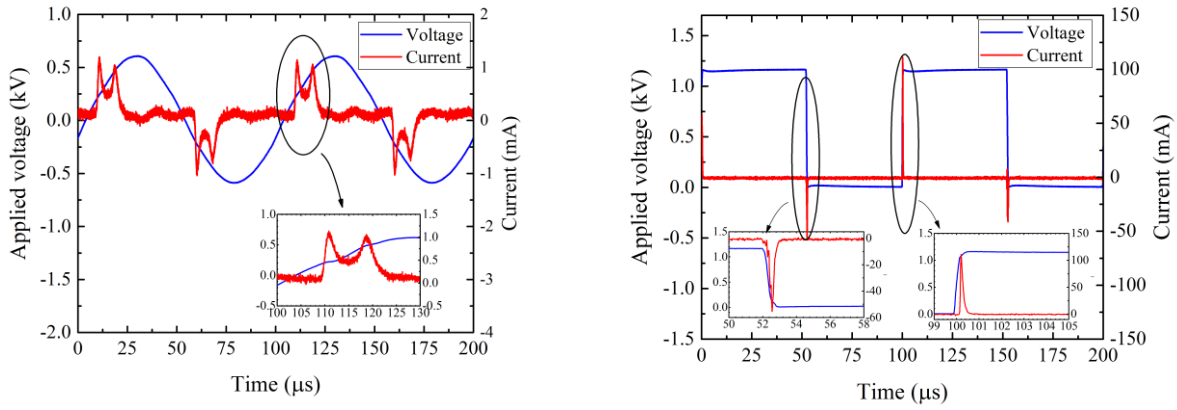

(a) sine-wave at V_{pp}=1.2kV. f=10kHz *(b) unipolar square-wave at V_{pp}=1.15kV.*

Figure 2: The typical voltage and current traces of DBDs driven by different waveforms.

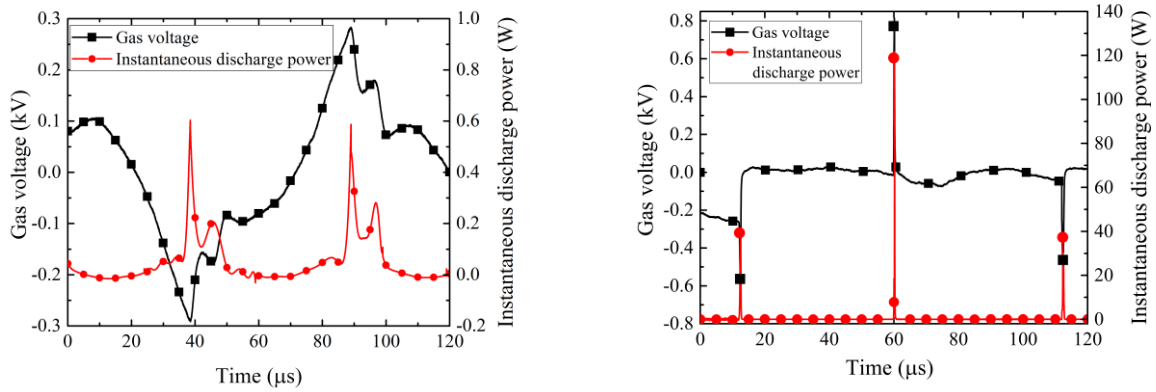

(a) sine-wave at V_{pp}=1.2kV. f=10kHz *(b) unipolar square-wave at V_{pp}=1.15kV. f=10kHz*

Figure 3: Applied voltage, gas voltage and power for of DBDs driven by different waveforms

A homogenous discharge was observed (confirmed by the current trace which had no evidence of streamers) in all the experiments regardless of waveform or applied peak-to-peak voltage. The discharge current for the sinusoidal excitation consists of two peaks per half cycle (1 mA and 0.8 mA), figure 2a. The origin of the second peak was due to the breakdown at the periphery of the discharge gap [26]. Small asymmetries were observed in the discharge current peaks but these can be explained by a difference in the electrode materials for the powered electrode (alumina) and the grounded electrode (stainless steel cone of the HPR-

60)[6, 26, 32]. The current density for the sinusoidal waveform varied from 0.1-0.8 mA/cm^2 with the duration of the current peak being 10-15 μs for V_{pp} between 0.9 kV-1.5 kV. The long discharge time, magnitude of the current densities and the fluctuation of V_{gas} over the entire sinusoidal cycle are clear evidence of atmospheric pressure Townsend discharge (APTD) mode (figure 3a) [6, 12]. The average power obtained for the sinusoidal excitation ranges from 39 to 94 mW, corresponding to an average discharge energy of ~4 μJ to ~9.5 μJ.

For the pulsed discharge, the peak current was significantly higher than the sinusoidal discharge, with the rising edge of the pulse producing 71 mA and the falling edge producing 39 mA (figure 2b). The difference in the current, for the rising and falling edges, was due to the difference in rise and fall times, 225 and 423 ns respectively. The current densities for the rising edge and falling edge were 10-50 mA/cm^2 and 10-20 mA/cm^2 respectively and these characteristics can be associated with the APGD mode [32, 33] . Further evidence of APGD mode can be observed by V_{gas} which was only present during the rising/falling pulse edge (figure 3b). For the pulsed discharge the average power was between 102 to 250 mW, corresponding to an average discharge energy of ~10 μJ to ~25 μJ. The average power dissipated in the pulse discharge increased to 1 W for voltages higher than 1.2 kV and the additional consumed power can be attributed to the arcing of the plasma which became visible around the circumference of the copper anode.

3. Results and Discussion

3.1 Neutral species

Prior to measurement of the ionic species a residual gas analysis of the DBD environment was carried out with the mass spectrometer tuned for helium. This was performed for a range of helium flow rates without a discharge present. At a flow rate of 2 slm the relative abundance of detected helium was 88.3% (figure 4). Other species in the working gas were found to be

N_2 4.3%, O_2 1.2%, H_2O 4.3% and CO_2 0.8% all originating from small amounts of ambient air in the discharge enclosure.

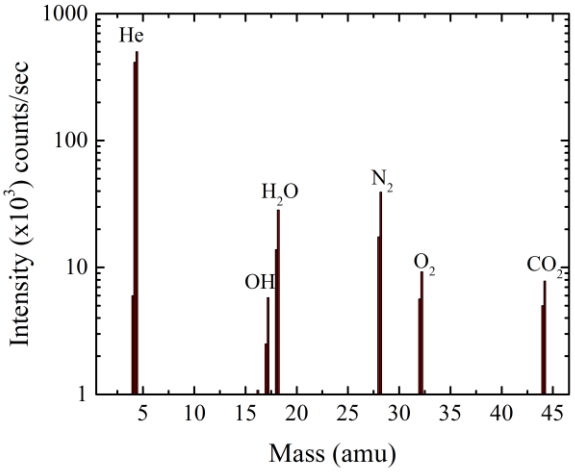

Figure 4. Mass spectra for neutrals present in helium a gas flow rate 2.0 slm

3.2 Positive ions

Time-averaged mass spectra of positive species in the DBD operating in both excitation modes were collected using the MBMS. No helium ions were directly detected in any of the discharges; this may be due to Penning ionization processes, dissociative excitation of water molecules and the short lifetimes of these species at atmospheric pressure [34]. Similar results have also been reported by Bruggeman et al [29] and Abd-Allah et al [27]. The relative abundance of the positive ions present in the APTD are shown in figure 5a (red is low power case (39 mW) and green is high power case (94 mW)). It can be seen that the APTD is primarily made up of molecular oxygen ions, low mass water vapor ions (H_2O^+), hydronium ions (H_3O^+) and nitrogen species for both power cases. As power was increased in the Townsend mode there was a small shift towards larger mass water vapor clusters. In the case of the APGD mode, figure 5b shows how the relative abundance of the ion species changed (red is low power mode (102 mW) and green is high power case (250 mW)). We observed low mass ions such as O_2^+ and N_2^+ become much less important and high mass water clusters

($H^+(H_2O)_4$) become the dominant species in the discharge. As we increased the power in this mode there was a small increase in the hydrated oxygen species.

Changes in water concentration within the discharge would typically explain the changes in positive ion chemistry that we observed, however, the ambient humidity was constant over the course of these experiments and the neutral species were monitored prior to ion extraction and no significant change was noticed, therefore this can be ruled out as a factor in the chemistry we observed. For that reason we must consider other factors which can influence the discharge chemistry.

The Townsend mode, as stated in the above section, has a lower current density that the glow mode, this can be attributed to a lower electron density (estimated from the current density to be ~$5x10^{10}$ cm^{-3}). It could also be assumed that due to the lower power deposited in the discharge that the average electron energy was also lower. From the average electric field (not shown here) this can be estimated to between ~ 1.7 eV and ~ 2 eV for the Townsend mode and ~3 to ~3.5 eV for the glow mode [35-37]. As a result of these factors ionization of species within the discharge will be reduced, with impurities/air species with the lowest ionization energy (molecular oxygen (12.06 eV), water (12.6 eV) and molecular nitrogen (15.58 eV)) becoming the dominant species.

Although this explains why molecular oxygen is dominant in the Townsend mode, it does not explain the large amount of water clusters, particularly $H^+(H_2O)_4$ in the glow mode. To explain this we look at two different factors, gas temperature and pulse off-time. Hydrated ions, $H^+(H_2O)_n$, are thought to be formed primarily by either Penning ionization of helium metastables or dissociation of water molecules [27], followed by a three body reaction process [38]. Hydration reactions are well documented to be gas temperature dependent, and due to the pulsed nature of the glow discharge, short on-time (when the current is high) and long off-time (no current detected), the gas temperature within the discharge is thought to vary significantly [39], in the case of the glow mode this temperature gradient is thought to enhance

the production of hydrated cluster ions. The long off-time of the pulse may also be a significant factor, providing sufficient time for more of these three-body reactions to occur and the large clusters to build up in the discharge.

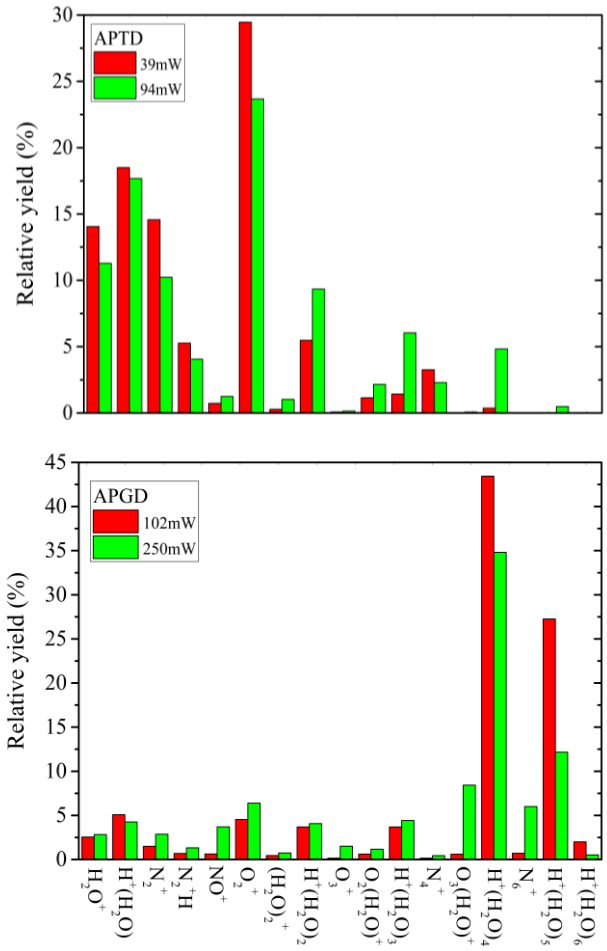

Figure 5 a) and 5b). Mass spectra for ions present in helium a gas flow rate 2.0 slm a) sinusoidal APTD for low and high power case and b) pulsed APGD for low and high power case.

While the relative abundance of these species changed with discharge mode it is important to note that the average number of counts the mass spectrometer detects is the approximately the same for O_2^+ in both discharge modes (the total number of counts/sec is higher in the glow mode compared to the Townsend mode), this suggests that additional chemical pathways become important in the glow mode. This may be due to the long-off time and temperature

gradient in the glow mode, and the low electron density and mean electron energy in the Townsend mode.

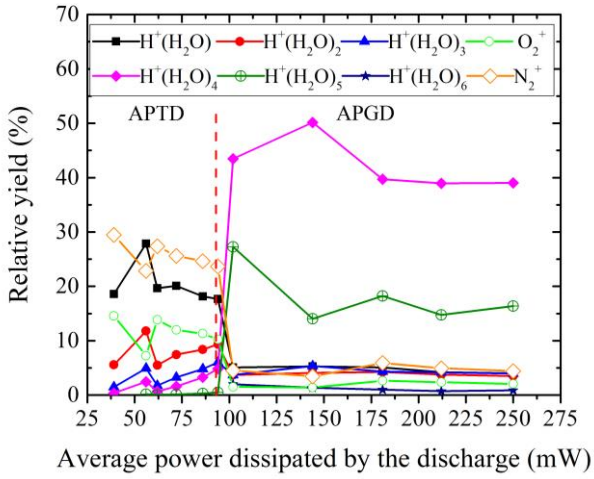

Figure 6) Relative abundance of the three main ion groups ($H^+(H_2O)_n$, O_2^+ and N_2^+) as a function of discharge power.

Figure 6 shows the trends of the main ions ($H^+(H_2O)_n$, O_2^+, and N_2^+) as a function of power, for both the Townsend and glow modes. From this we can see a clear transition in the chemistry as the discharge mode changes from Townsend to glow. For $H^+(H_2O)_4$ we see a 40% increase in the relative abundance of this cluster in the discharge, but the change is not the same for all species, for example we only see a 10% reduction in H_3O^+. As this species is

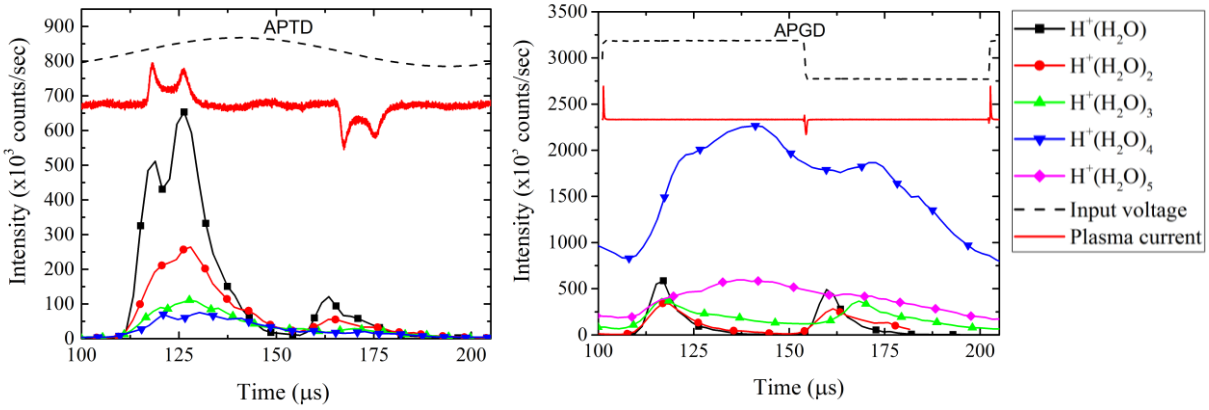

Figure 7a) and 7b). Time-resolved mass spectrometry data of water cluster ions a) APTD, and b) APGD

key to cluster formation we would expect this change to be proportional to each other with small species decreasing to feed the three-body hydration reaction. This may suggest that more H_3O^+ is being produced at certain periods within the pulsed glow mode cycle, which is then consumed to produce the larger cluster. To investigate this hypothesis we investigated the two discharge modes using time-resolved MS (time-step of 2 μs with a gated window duration of 3 μs). This allowed us to examine how the postive ion chemistry changed on microsecond timescales and relate this to the voltage and current waveforms. Figure 7 shows the trends of the $H^+(H_2O)_n$ ions as a fuction of time. From this we can see that the maximum H_3O^+ production occurred just after the current peak, in both discharge modes, but the production for the Townsend mode happens over ~40 μs and the second production period has a significantly reduced maximum. In the glow mode however the production period was much shorter, ~15 μs, but the second production phase achieves the same maximum as the first. Time-averaged data misses these differences and shows that overall production was the same. For the larger clusters, it is clear that in the glow mode these species were formed in the long off-phase of the pulse, with the second current peak initiating significant loss mechanisms, however a clear buildup of $H^+(H_2O)_4$ can be seen, this was carried over to subsequent pulses. As other large clusters do not show the same level of persistance in the pulsed discharge this suggests that formation time, formation location and temperature may be a key factor in these reactions.

3.3 Negative ions

Figure 8a and 8b display the negative ion content for the same low power and high power cases shown for the positive ions, for both the APTD and APGD modes. The negative ion content of the APGD is much more diverse than that of the APTD, as was the case for the positive ions. Similar negative ion mass spectra have also been observed in other atmospheric pressure plasmas [22, 24]. The negative ions are mainly generated by dissociative electron

attachment. The main negative ion in the low power case of the APTD is atomic oxygen (O^-), as power is increased nitrogen oxides and hydrated nitrogen oxide (NO_2^- and $NO_2^-(H_2O)$) becomes more important. This is thought to be due to the mean electron energy in the discharge increasing to a level where nitrogen dissociation reactions become important, leaving free bonding sites for oxygen anion attachment.

The trends as a function of power for the main anions for APGD and APTD are presented in figure 9. For APGD the main ions in the low power cases are the hydrated nitric oxide species ($NO_2^-(H_2O)$ and $NO_2^-(H_2O)_2$), these species were also important in the high power APTD

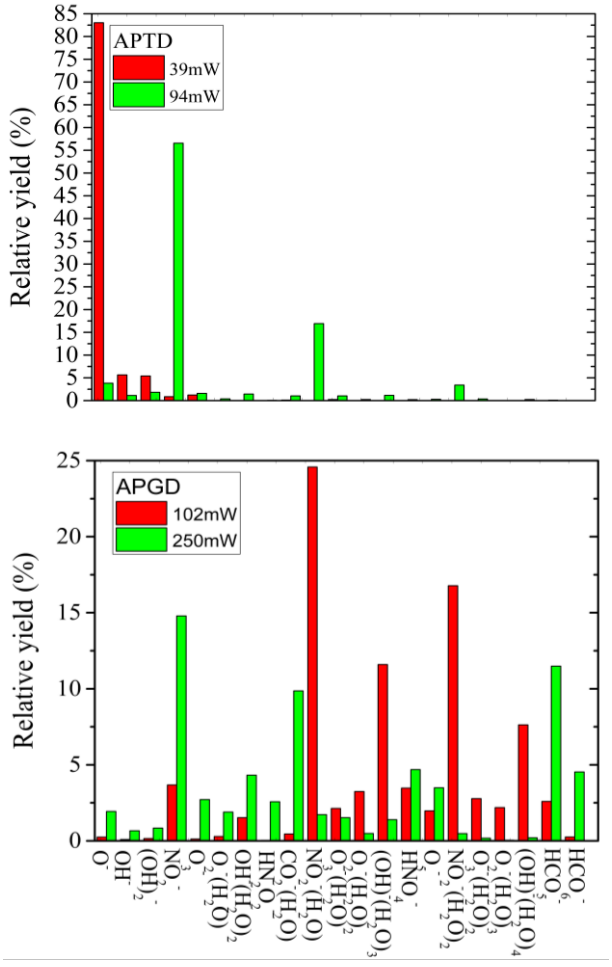

Figure 8 a) and 8b). Mass spectra for negative ions present in helium a gas flow rate 2.0 slm a) sinusoidal APTD for low and high power case and b) pulsed APGD for low and high power case.

case. This suggests that the increased power or large temperature gradients may enhance the hydration reactions processes; this is consistent with the results shown for the positive ions under different conditions. For the high power APGD case the negative ions appear to revert to a less hydrated state and NO_2^- species become more abundant in the discharge. These higher powers seem to result in a change of mean electron energy in the off-phase of the glow mode, resulting in different attachment and loss pathways becoming important in the discharge.

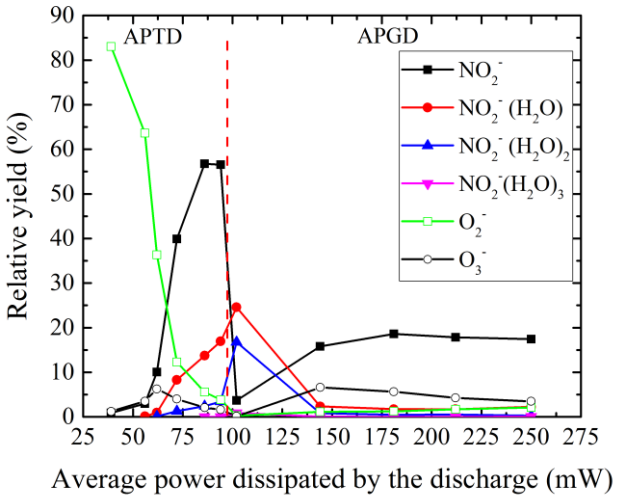

Figure 9: Relative abundance of the main negative ions as a function of discharge power

4. Conclusions

Using molecular beam mass spectrometry, the positive and negative ion chemistry of a DBD operating in either glow or Townsend discharge regimes has been studied. The experimental results reveal a change in the positive ions produced with large protonated water clusters generated in APGD mode, and relatively small molecular ions produced in APTD mode. Homogenous operation in the APGD mode was made possible through the use of microsecond square wave pulsed with nanosecond rise and fall times, pulsed operation of the discharge is thought to be a significant contributing factor to the changes in chemistry between the two modes. The dominant ions observed in the APTD were molecular oxygen ions, hydronium (H_3O^+) and nitrogen species, whereas for the APGD high mass water clusters

($H^+(H_2O)_4$) dominate. It is suggested, in this paper, that the shift in dominant species may be due to a change in chemical pathways and reaction rates caused by a change in electron density and mean electron energy, gas temperature and long off-times in the pulsed glow mode.

For the negative ions a similar pattern can be found with a shift away from small ions towards larger hydrated ions as power was increased, however, as power was increased further in the APGD mode, we see a shift back towards less hydrated species and a larger range of negative air species. This trend can also be seen with the positive ions, but it is less pronounced. This shift away from hydrated species is thought to be due to a change of gas temperature, for the high power APGD a temperature gradient will still be produced due to the pulsed nature of the discharge, however the increase in power will give the discharge a higher overall temperature than the low power case, which is less favorable for hydration reactions. A shift in electron energy distribution may also influence the chemical pathways, and enhance additional electron attachment pathways for other air molecules.

Acknowledgements: The authors would like to thank the Chinese Scholarship Council for funding Dr. He's salary during the project

Received: ((will be filled in by the editorial staff)); Revised: ((will be filled in by the editorial staff)); Published online: ((please add journal code and manuscript number, e.g., DOI: 10.1002/ppap.201100001))

Keywords: dielectric barrier discharges; molecular beam mass spectrometry; atmospheric-pressure plasma; nanosecond pulsing; plasma chemistry

References

1. Daeschlein, G., et al., *Skin decontamination by low-temperature atmospheric pressure plasma jet and dielectric barrier discharge plasma.* Journal of Hospital Infection, 2012. **81**(3): p. 177-183.
2. Wang, Q., et al., *Low-temperature plasma synthesis of carbon nanotubes and graphene based materials and their fuel cell applications.* Chemical Society Reviews, 2013. **42**(23): p. 8821-8834.
3. Liu, C., N.M.D. Brown, and B.J. Meenan, *Dielectric barrier discharge (DBD) processing of PMMA surface: Optimization of operational parameters.* Surface and Coatings Technology, 2006. **201**(6): p. 2341-2350.
4. Pal, U.N., et al., *Analysis of Discharge Parameters in Xenon-Filled Coaxial DBD Tube.* Ieee Transactions on Plasma Science, 2011. **39**(6): p. 1475-1481.
5. Moreau E., D.A., Benard N., Jukes T. ,Whallety R.,Choi K.,Berendt A.,Podlinski J.,Mizeraczyk J., *Surface dielectric Barrier Discharge Plasma Actuators.* ERCOFTAC Bulletin, 2013(94): p. 5-10.
6. Bogaczyk, M., G.B. Sretenovic, and H.E. Wagner, *Influence of the applied voltage shape on the barrier discharge operation modes in helium.* European Physical Journal D, 2013. **67**(10).
7. Rajasekaran, P., et al., *Filamentary and Homogeneous Modes of Dielectric Barrier Discharge (DBD) in Air: Investigation through Plasma Characterization and Simulation of Surface Irradiation.* Plasma Processes and Polymers, 2010. **7**(8): p. 665-675.
8. Kogelschatz, U., *Dielectric-barrier discharges: Their history, discharge physics, and industrial applications.* Plasma Chemistry and Plasma Processing, 2003. **23**(1): p. 1-46.
9. Golubovskii, Y.B., et al., *Modelling of the homogeneous barrier discharge in helium at atmospheric pressure.* Journal of Physics D-Applied Physics, 2003. **36**(1): p. 39-49.
10. Shao, T., et al., *Temporal evolution of nanosecond-pulse dielectric barrier discharges in open air.* Epl, 2012. **97**(5).
11. Shao, T., et al., *A Comparative Study of Water Electrodes Versus Metal Electrodes for Excitation of Nanosecond-Pulse Homogeneous Dielectric Barrier Discharge in Open Air.* Ieee Transactions on Plasma Science, 2013. **41**(10): p. 3069-3078.
12. Massines, F., et al., *Glow and Townsend dielectric barrier discharge in various atmosphere.* Plasma Physics and Controlled Fusion, 2005. **47**(12 B): p. B577-B588.
13. Massines, F., et al., *Recent advances in the understanding of homogeneous dielectric barrier discharges.* European Physical Journal-Applied Physics, 2009. **47**(2).
14. Choi, J.H., et al., *Investigation of the transition between glow and streamer discharges in atmospheric air.* Plasma Sources Science & Technology, 2006. **15**(3): p. 416-420.
15. Liu, S. and M. Neiger, *Excitation of dielectric barrier discharges by unipolar submicrosecond square pulses.* Journal of Physics D: Applied Physics, 2001. **34**(11): p. 1632-1638.
16. Liu, S.H. and M. Neiger, *Double discharges in unipolar-pulsed dielectric barrier discharge xenon excimer lamps.* Journal of Physics D-Applied Physics, 2003. **36**(13): p. 1565-1572.

17. McKay, K., et al., *Mass spectrometric diagnosis of an atmospheric pressure helium microplasma jet.* Journal of Physics D-Applied Physics, 2013. **46**(46).
18. Yue, Y., et al., *Study of dielectric barrier townsend Discharge in air at atmospheric pressure*, in *Pulsed Power Conference 19th IEEE*. 2013.
19. Starostin, S.A., et al., *On the formation mechanisms of the diffuse atmospheric pressure dielectric barrier discharge in CVD processes of thin silica-like films.* Plasma Sources Science & Technology, 2009. **18**(4).
20. Luo, H.Y., X.X. Wang, and C.R. Li, *Extraordinary extinction of dielectric barrier Townsend discharge in nitrogen at atmospheric pressure.* Epl, 2012. **97**(1).
21. Tay, W.H., S.L. Yap, and C.S. Wong, *Electrical Characteristics and Modeling of a Filamentary Dielectric Barrier Discharge in Atmospheric Air.* Sains Malaysiana, 2014. **43**(4): p. 583-594.
22. Oh, J.S., Y. Aranda-Gonzalvo, and J.W. Bradley, *Time-resolved mass spectroscopic studies of an atmospheric-pressure helium microplasma jet.* Journal of Physics D-Applied Physics, 2011. **44**(36).
23. Hung, C.T., et al., *Investigation of the Atmospheric Helium Dielectric Barrier Discharge Driven by a Realistic Distorted-Sinusoidal Voltage Power Source.* Plasma Chemistry and Plasma Processing, 2011. **31**(1): p. 1-21.
24. Oh, J.S., et al., *Investigating the effect of additional gases in an atmospheric-pressure helium plasma jet using ambient mass spectrometry.* Japanese Journal of Applied Physics, 2015. **54**(1).
25. Muller, S., et al., *Operation modes of the helium dielectric barrier discharge for soft ionization.* Spectrochimica Acta Part B-Atomic Spectroscopy, 2013. **85**: p. 104-111.
26. R. Foest, V.A.M., Yu. B. Golubovskii, J. F. Behnke, M. Schmidt, *Study of a Helium Atmospheric Pressure Dielectric Barrier Discharge at 100 kHz*, in *International Conference on Phenomena in Ionized Gases [26th]*. 2003: Germany.
27. Abd-Allah, Z., et al., *Mass spectrometric investigation of the ionic species in a dielectric barrier discharge operating in helium-water vapour mixtures.* Journal of Physics D-Applied Physics, 2015. **48**(8).
28. Chiper, A.S., et al., *A Comparative Study of helium and argon DBD plasmas suitable for thermosensitive materials processing* Romanian Journal of Physics, 2011. **56**: p. 126-131.
29. Bruggeman, P., et al., *Mass spectrometry study of positive and negative ions in a capacitively coupled atmospheric pressure RF excited glow discharge in He-water mixtures.* Journal of Physics D-Applied Physics, 2010. **43**(1).
30. Grosse-Kreul, S., et al., *Mass spectrometry of atmospheric pressure plasmas.* Plasma Sources Science & Technology, 2015. **24**(4).
31. Shao, T., et al., *Experimental study on repetitive unipolar nanosecond-pulse dielectric barrier discharge in air at atmospheric pressure.* Journal of Physics D-Applied Physics, 2008. **41**(21).
32. Li, X.C., et al., *Characteristics of an atmospheric pressure argon glow discharge in a coaxial electrode geometry.* Plasma Sources Science & Technology, 2008. **17**(1).
33. Golubovskii, Y.B., et al., *Influence of interaction between charged particles and dielectric surface over a homogeneous barrier discharge in nitrogen.* Journal of Physics D-Applied Physics, 2002. **35**(8): p. 751-761.
34. Liu, D.X., et al., *Global model of low-temperature atmospheric-pressure He + H2O plasmas.* Plasma Sources Science & Technology, 2010. **19**(2).
35. Deng, X.T. and M.G. Kong, *Frequency range of stable dielectric-barrier discharges in atmospheric He and N-2.* Ieee Transactions on Plasma Science, 2004. **32**(4): p. 1709-1715.

36. Brunger, M.J., et al., *Differential cross-sections for elastic and inelastic N=2 excitation of ground-state helium at29.6 and 40.1eV* Journal of Physics B-Atomic Molecular and Optical Physics, 1990. **23**(8): p. 1325-1335.
37. Fridman, A., *Plasma chemistry*. 2008, Cambridge university press.
38. Murakami, T., et al., *Chemical kinetics and reactive species in atmospheric pressure helium-oxygen plasmas with humid-air impurities.* Plasma Sources Science & Technology, 2013. **22**(1).
39. Roettgen, A., et al., *Time-resolved electron density and electron temperature measurements in nanosecond pulse discharges in helium.* Plasma Sources Science & Technology, 2016. **25**(5).